



Looking inside an endohedral fullerene: Inter- and intramolecular ordering of $\text{Dy}_3\text{N} @ \text{C}_{80} (I_h)$ on Cu(111)

Matthias Treier,^{1,*} Pascal Ruffieux,¹ Roman Fasel,¹ Frithjof Nolting,² Shangfeng Yang,^{3,4}
Lothar Dunsch,³ and Thomas Greber⁵

¹*Empa, Swiss Federal Laboratories for Materials Testing and Research, nanotech@surfaces Laboratory, 3602 Thun and 8600 Dübendorf, Switzerland*

²*Swiss Light Source, Paul Scherrer Institut, 5232 Villigen PSI, Switzerland*

³*Leibniz Institute for Solid State and Materials Research, 01069 Dresden, Germany*

⁴*Hefei National Laboratory for Physical Sciences at Microscale and Department of Materials Science and Engineering, University of Science and Technology of China, Hefei 230026, China*

⁵*Physics Institute, University of Zurich, 8057 Zurich, Switzerland*

(Received 24 June 2009; revised manuscript received 22 July 2009; published 11 August 2009)

The inter- and intramolecular ordering of the trimetallic nitride endohedral fullerene $\text{Dy}_3\text{N} @ \text{C}_{80}$ with icosahedral cage symmetry I_h on Cu(111) has been studied by scanning tunneling microscopy and synchrotron-based x-ray photoelectron diffraction (XPD). $\text{Dy}_3\text{N} @ \text{C}_{80} (I_h)$ is found to form ordered islands consisting of domains of equally oriented molecules. As for C_{60} on the same substrate, the cage is facing with a hexagon toward the surface, which is however slightly tilted for C_{80} . The endohedral nitrogen atom remains at a position close to the geometrical center of the cage. Resonant XPD on the M_V edge shows that the encaged Dy_3N unit takes well-defined orientations with respect to the C_{80} cage and the Cu(111) substrate.

DOI: [10.1103/PhysRevB.80.081403](https://doi.org/10.1103/PhysRevB.80.081403)

PACS number(s): 68.35.bp, 61.05.js, 68.37.Ef, 68.43.Fg

Metal-containing endohedral fullerenes have attracted great interest over the last decade due to their unique electronic properties associated with the charge transfer from the endohedral metal complex to the carbon cage. Endohedral fullerenes exhibit a variety of novel properties such as peculiar redox- and electrochemical behavior, and luminescence and nonlinear optical response.¹ Furthermore, they represent an interesting class of materials since they offer the opportunity to study and possibly manipulate small clusters of endohedral atoms, which might, for example, be applied in future information storage devices. Due to the comparably high production yields that can be achieved, research on endohedral trimetallic nitride cluster (TNT) fullerenes^{2,3} has increased in recent years.^{2,4–7} TNT endohedral fullerenes have been shown to possess an endohedral ordering in condensed phases such as cocrystals.^{5,8} They have also been shown to possess unique magnetic properties,^{7,9} motivating their application in future memory storage devices. For such applications, ordered arrays of endohedral units and the possibility to switch the orientation of the endohedral units to store information are required. The self-assembly of TNT endohedral fullerenes on surfaces has been analyzed previously by scanning tunneling microscopy (STM).^{10–12} However, these studies have not addressed the issue of endohedral ordering in the adsorbed state since this information is not accessible by STM studies alone. On the other hand, the position of the metal atom with respect to the cage of single-atom endohedral metallofullerenes has been studied by x-ray standing-wave techniques,^{13,14} without however simultaneously addressing the orientation of the cage.

In this Rapid Communication we present a detailed study of (sub-)monolayers of the endohedral trimetallic nitride cluster fullerene $\text{Dy}_3\text{N} @ \text{C}_{80} (I_h)$ (Ref. 6) on Cu(111) (see Fig. 1). We show that the combination of STM and both standard and resonant x-ray photoelectron diffraction (rXPD) allows for a determination of the inter- and intramolecular

ordering. We find that $\text{Dy}_3\text{N} @ \text{C}_{80} (I_h)$ forms an ordered superstructure on this template, with both the cage and the endohedral unit being ordered with respect to the substrate.

Angle-scanned x-ray photoelectron-diffraction experiments were performed at the NearNode endstation of the SIM beamline at the Swiss Light Source. Low-temperature STM (LT-STM) measurements were conducted using an Omicron LT-STM. Both systems were operated at ultra high-vacuum conditions with base pressure below 2×10^{-10} mbar. $\text{Dy}_3\text{N} @ \text{C}_{80} (I_h)$ has been deposited from resistively heated quartz/diamondlike carbon coated steel crucibles held at about 770 K onto the sample, which was held at room temperature. The substrate has been cleaned by standard Ar^+ -ion sputtering/annealing cycles prior to deposition of the endohedral fullerene. XPD has been performed at room temperature while STM data were acquired at 77 K.

STM measurements¹⁵ of submonolayers of $\text{Dy}_3\text{N} @ \text{C}_{80} (I_h)$ on Cu(111) show that islands of the adsorbate grow out from step edges on both the lower and upper terraces adjacent to the step. Locally, the orientation of the superstructures follows the orientation of the step edges as shown in Fig. 2(a). However, low-energy electron diffraction (LEED) shows that at higher coverage (close to a complete monolayer), a $(\sqrt{19} \times \sqrt{19})R \pm 23.4^\circ$ dominates with no other su-

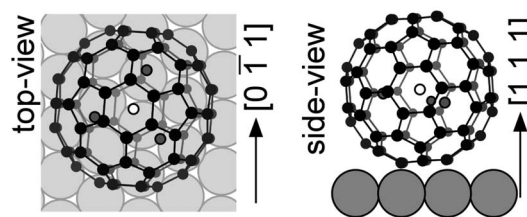


FIG. 1. Model of $\text{Dy}_3\text{N} @ \text{C}_{80} (I_h)$ adsorbed on Cu(111). Carbon atoms are shown in grayscale, while small white/gray filled circles correspond to endohedral nitrogen/dysprosium atoms.

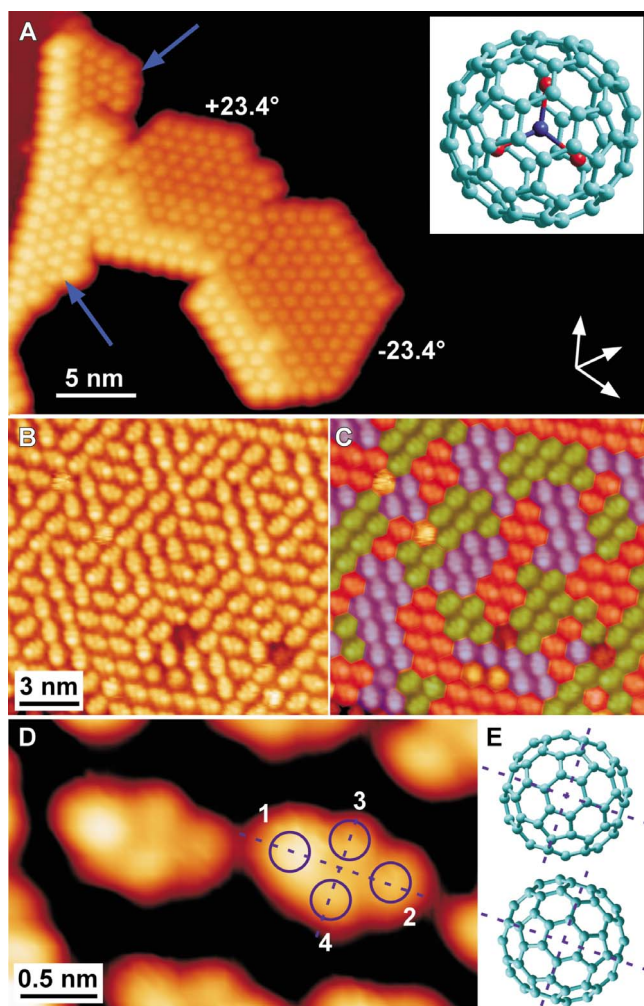


FIG. 2. (Color online) STM images of $\text{Dy}_3\text{N}@C_{80}(I_h)$ on $\text{Cu}(111)$. (a) Overview image showing the correlation between the overlayer structure and the local step edge direction. Arrows point to small patches of adsorbates, which adopt a superstructure different from the dominant $\sqrt{19}$ superstructure. (b) Intramolecular contrast resolved STM image of a $+23.4^\circ$ island showing the formation of small domains of equally oriented molecules within an island. (c) Visualization of domains; colored (grayscale) STM image of the area shown in (b). (d) High-resolution STM image of two molecules, showing intramolecular contrast. Four protrusions per molecule can be identified. (e) Suggested models of C_{80} cage orientation compatible with the symmetry of the intramolecular features from (d). Dashed lines correspond to the symmetry elements from (d). [Scanning parameters: (a) 80 pA, -1.8 V (B,C,D) 0.3 nA, -0.1 V.]

perstructures spanning over dimensions to be visible in LEED. The nearest-neighbor distances in the other superstructures are—within the measurement error of STM—equal to the ones within the long-range-ordered superstructure (1.1 nm). High-resolution STM images show that within islands of the $\sqrt{19}$ superstructure, three rotationally equivalent molecular orientations are found. Equally oriented molecules form small domains of typically 5–15 molecules within larger islands as shown in Figs. 2(b) and 2(c).

A high-resolution image with clearly resolved intramolecular structure is shown in Fig. 2(d). Four protrusions per

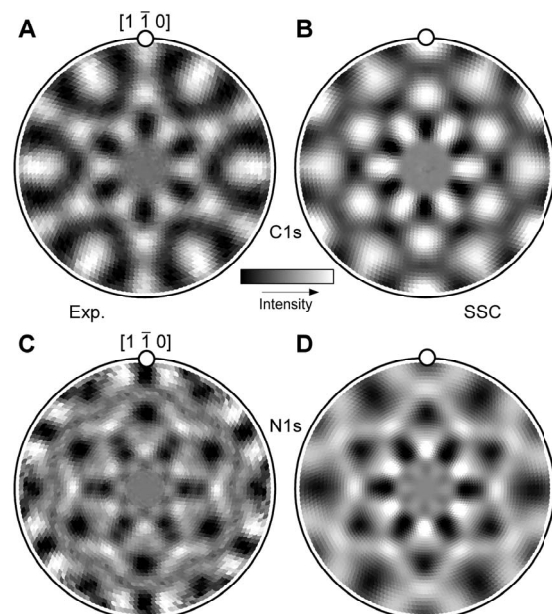


FIG. 3. Synchrotron radiation XPD ($h\nu=880$ eV) patterns of 1ML of $\text{Dy}_3\text{N}@C_{80}(I_h)$ on $\text{Cu}(111)$. (a) Experimental C 1s-XPD. (b) Best-fit C 1s-SSC. (c) Experimental N 1s-XPD. (d) Best-fit N 1s-SSC.

molecule can be discerned. While the protrusions labeled 3 and 4 approximately have the same apparent height, this is not the case for protrusions 1 and 2, with protrusion 1 appearing $0.2\text{--}0.3$ Å higher. The particular intramolecular contrast cannot be readily related to a molecular-orbital or structural elements of the cage. However, it is possible to derive possible adsorption orientations of the cage based on symmetry considerations. The molecule appears to be symmetric with respect to the dashed lines passing through maxima 1 and 2 [Fig. 2(d)] while the difference in apparent height can be explained by a rotation of the cage around the axis represented by the dashed line passing through maxima 3 and 4. Such a rotation would correspond to a tilt of the cage with respect to a highly symmetric adsorption geometry. Two adsorption geometries compatible with these symmetry considerations are given in Fig. 1(e) with the cage facing toward the surface with a hexagon in both cases. Since electronic and geometric effects cannot be clearly separated by STM, a quantitative analysis of this tilt and unambiguous determination of the adsorption geometry is not possible by STM alone. In particular, STM does not yield information on the endohedral ordering. We have therefore complemented the STM results by an XPD study, a combination of techniques, which has previously been shown to allow for a determination of the three-dimensional orientation of large organic adsorbates.¹⁶

C 1s- and N 1s-XPD patterns are shown in Figs. 3(a) and 3(c). The C 1s-XPD pattern [Fig. 3(a)] of a monolayer of $\text{Dy}_3\text{N}@C_{80}(I_h)$ bears some resemblance to the corresponding pattern produced by a monolayer of C_{60} on the same substrate.¹⁷ However, the pattern produced by the C_{80} cage is rotated azimuthally by 30° compared to the case of C_{60} , directly indicating that the adsorption orientation must be different for this type of fullerene. The large number of in-

equivalent emitter-scatterer directions is directly reflected in the broad shape of the maxima. Due to the single photoelectron emitter per molecule, the N 1s photoelectron-diffraction pattern [Fig. 3(c)] is highly anisotropic ($\sim 20\%$). It is therefore possible to measure clearly distinguishable diffraction features even at this low nitrogen concentration of only about ~ 1 atom/nm² within the Dy₃N@C₈₀(I_h) monolayer. Single scattering cluster (SSC) simulations¹⁸ have been used to find the molecular orientation yielding the lowest reliability factor (*R* factor) and hence the best agreement with experiment.¹⁹ Backscattering from substrate atoms has been neglected since the backscattering yield is very low within the kinetic-energy range used for this work (>400 eV).

From both the C 1s- and the N 1s-XPD patterns, it is found that, similar to C₆₀, the C₈₀ cage is facing toward the surface with a hexagon. However, the exact orientation of the hexagon in C₈₀ differs from the one determined for C₆₀. As mentioned in the previous section, STM stipulates an out-of-plane rotation of the cage which is confirmed by XPD.²⁰ The best fit with experiment is obtained for a tilt angle ψ of the hexagon face of $3^\circ \pm 2^\circ$ with respect to the (111) plane of the substrate and an azimuthal orientation $\phi = 4^\circ \pm 2^\circ$, which compares well with the STM result from which ϕ can be estimated to about $6^\circ \pm 6^\circ$. Figure 1 illustrates this best-fit orientation of the C₈₀ cage. Only the cage orientation shown in the bottom part of Fig. 2(e) is thus compatible with XPD. The alternative model derived from STM [upper part of Fig. 2(e)] can be excluded based on the SSC analysis. We note that the *R* factor has a shallow minimum around this adsorption configuration which is reflected in the relatively large error associated with the cage orientation. We have however also independently determined the cage orientation from the N 1s-XPD data, and the same orientational angles were found to give the lowest *R* factor, suggesting that the actual error is smaller than the value quoted above. The position of the endohedral nitrogen atom in the direction orthogonal to the surface has also been determined by SSC. It is found that the nitrogen atom remains at a position close to the center of the C₈₀ cage also in the adsorbed state (Fig. 1). A pronounced minimum is found for a position of the nitrogen atom at 0.1 ± 0.2 Å below the geometrical center of the cage. As can be seen by comparing Figs. 3(a)–3(d), respectively, the agreement between simulated and measured diffraction patterns is excellent for both C 1s and N 1s patterns.

While C 1s and N 1s photoelectron-diffraction patterns of excellent quality could be measured by standard synchrotron-based angle-scanned XPD, similar recording of Dy 4*d* patterns proved unsuccessful. The large number of final states leads to a significant broadening of the Dy 4*d* peak²¹ resulting in a low peak-to-background ratio. In conjunction with the strongly anisotropic secondary electron background (due to the close-lying Cu 3*s* photoelectron peak) this prevents a clear assignment of diffraction features to Dy 4*d* photoelectrons. In order to increase the peak-to-background ratio we used rXPD.^{22,23} Here this technique is exploited to enhance the signal-to-background ratio of Dy emitters. The signal at a given energy is proportional to the ratio between the cross section and the line width. As outlined above, the broad Dy 4*d* multiplet inhibits the observation of off-resonance Dy 4*d* XPD patterns, although the

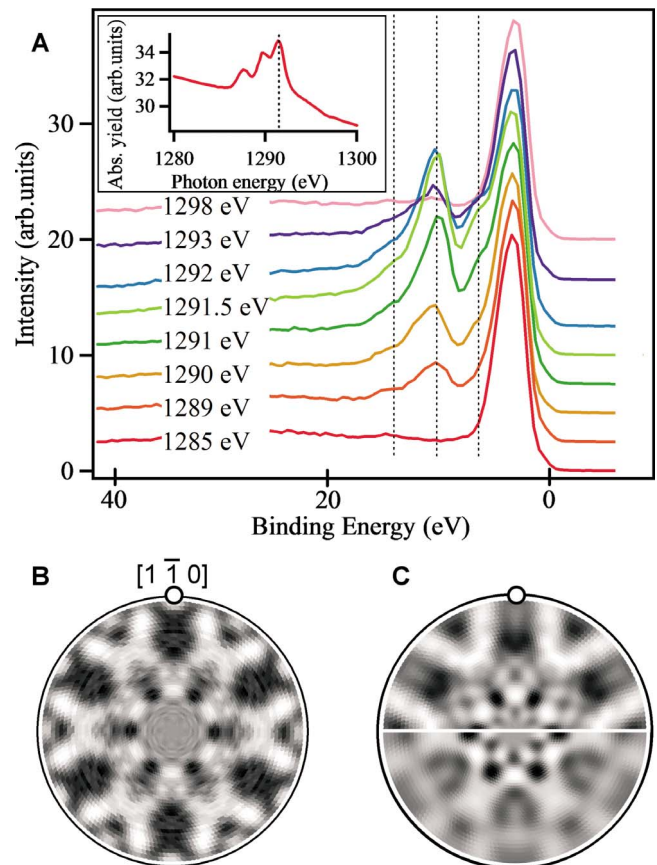


FIG. 4. (Color online) rXPD of Dy-*MNN* Auger lines. (a) Resonant enhancement of Auger lines (dotted lines) as a function of photon energy. The inset shows the corresponding x-ray absorption spectrum across the Dy *M_V* edge (3*d*). The dashed line designates the photon energy of 1291.5 eV. (b) Dy-*MNN*-rXPD of IML Dy₃N@C₈₀(I_h) on Cu(111), recorded at a photon energy of 1291.5 eV. (c) Best-fit SSC simulation (upper half, see text for details) and simulation based on disordered endohedral unit (lower half).

Dy 4*d* photoemission cross section is significantly larger than that of N 1s. Resonant excitation of the Dy 3*d*-4*f* transition enhances the cross section to linewidth ratio by more than 2 orders of magnitude. As shown below, the angular modulation of the corresponding Auger-electron emission allows for the acquisition of statistically significant Dy-related diffraction data.

The inset in Fig. 4(a) shows the x-ray absorption spectrum of one monolayer of Dy₃N@C₈₀(I_h) on Cu(111). It corresponds to that of trivalent Dy and peaks at about 1291 eV photon energy,²⁴ where the *MN* absorption and subsequent electron emission with a kinetic energy of 1281 eV are highest. Figure 4(a) shows the dependence of the electron emission intensity on the photon energy. The Cu 3*d* substrate valence band emission remains constant at a binding energy of 4 eV, as does the resonant Dy-*MNN* emission at 10.5 eV binding energy. This indicates that most of the emission is due to Auger resonant Raman de-excitation, where the photoexcited electron still resides on the Dy atom while it de-excites and not due to a regular Auger de-excitation that is independent of the photon energy.²⁵ However, both of these Auger emission processes are expected to have localized

electron source waves that are a prerequisite for the interpretation of angle-scanned electron-diffraction data, and we may thus make use of their greatly enhanced signal-to-background ratio.

Figure 4(b) shows a rXPD pattern recorded at a photon energy of 1291.5 eV on the strongest Dy-MNN Auger feature. The ordering of the fullerene cages as evidenced by the data in Fig. 3 also imposes a diffraction pattern with sizable contrast for Dy emitters that are randomly distributed on a sphere inside the carbon cage [see lower half of Fig. 4(c)]. The unsatisfactory *R* factor and small anisotropy of this simulation do however clearly exclude this possibility. This infers that there exists order between the cage and the endohedral units. Further SSC simulations show that this endohedral ordering is different from the one found in bulk phases.^{8,20} It must therefore be concluded that the endohedral Dy₃N unit “feels” the underlying Cu(111) surface and adopts suitable orientations.

To investigate further on the orientation of the endohedral Dy₃N unit, the experimental Dy-rXPD pattern has been compared to a series of SSC simulations based on different model systems, considering both planar and pyramidal endohedral units. A slight deviation from planarity in bulk crystals has been suggested in the literature⁸ but smaller (<0.1 Å) than for other endohedral trimetallic nitride cluster fullerenes.⁵ Details on the SSC simulations can be found elsewhere.²⁰ To summarize these simulations, we find that a single orientation for the endohedral unit is not sufficient to reproduce the experimental Dy-rXPD pattern. Also, it is not possible to clearly evidence or exclude a possible pyramidalization of the endohedral unit. However, two coexisting endohedral configurations—one with a planar unit inclined with respect to the (111) surface and a slightly pyramidal one approximately parallel to the surface—satisfactorily reproduce the experiment. The corresponding best-fit Dy-SSC calculation is shown in Fig. 4(c) (upper half). Also with this

pattern that assumes endohedral Dy₃N units with different conformations, the agreement between simulation and experiment is not as good as for the N 1s and C 1s patterns with the *R* factor being approximately 30% larger. Since an isotropic distribution of the endohedral atoms can be excluded [Fig. 4(c) lower half] it can nevertheless be concluded that the endohedral unit adopts its orientation to the presence of the underlying surface, resulting in more than one coexisting orientations of the endohedral unit in the adsorbed state. This is in line with several coexisting orientations of the latter within cocrystals.^{5,8,26,27}

With the large variety of currently available multiatom endohedral fullerenes,²⁸ the adsorption of such endohedral fullerenes on single-crystal surfaces provides a means to create ordered arrays of endohedral decoupled clusters, which might be oriented by application of external fields. The present study has shown that monolayer-thick ordered arrays of endohedral fullerenes can be grown and characterized on single-crystal surfaces, opening the way for future experiments exploring these ideas which would be relevant for nanoscale information storage.

In summary, we have shown that the endohedral fullerene Dy₃N@C₈₀ (*I_h*) adsorbs on Cu(111) in a way that at monolayer coverage, both the cage and the endohedral unit are ordered. The C₈₀ cage faces toward the surface with a hexagon whose plane is slightly tilted with respect to the substrate. The look inside the endohedral fullerene indicates that the nitrogen remains near the center of the cage and the endohedral Dy₃ unit takes at least two inequivalent orientations in the C₈₀ cages on the substrate surface.

Financial support from the Swiss National Science Foundation and the NCCR “nanoscale science” is gratefully acknowledged. Parts of these experiments were performed on the SIM beamline at the Swiss Light Source, Paul Scherrer Institut, Villigen, Switzerland.

*Author to whom correspondence should be addressed; matthias.treier@gmail.com

¹H. Shinohara, Rep. Prog. Phys. **63**, 843 (2000).

²S. Stevenson *et al.*, Nature (London) **401**, 55 (1999).

³L. Dunsch, M. Krause, J. Noack, and P. Georgi, J. Phys. Chem. Solids **65**, 309 (2004).

⁴L. Alvarez *et al.*, Phys. Rev. B **66**, 035107 (2002).

⁵S. Stevenson *et al.*, Chem. Commun. (Cambridge) **2004**, 2814.

⁶S. F. Yang and L. Dunsch, Chem.-Eur. J. **12**, 413 (2006).

⁷M. Wolf *et al.*, Angew. Chem., Int. Ed. **44**, 3306 (2005).

⁸S. F. Yang *et al.*, J. Am. Chem. Soc. **128**, 16733 (2006).

⁹M. Wolf *et al.*, J. Magn. Magn. Mater. **290–291**, 290 (2005).

¹⁰D. F. Leigh *et al.*, Surf. Sci. **601**, 2750 (2007).

¹¹D. S. Deak, F. Silly, K. Porfyrakis, and M. R. Castell, J. Am. Chem. Soc. **128**, 13976 (2006).

¹²D. S. Deak, F. Silly, K. Porfyrakis, and M. R. Castell, Nanotechnology **18**, 075301 (2007).

¹³C. Ton-That *et al.*, Phys. Rev. B **68**, 045424 (2003).

¹⁴R. A. J. Woolley *et al.*, Nano Lett. **4**, 361 (2004).

¹⁵I. Horcas *et al.*, Rev. Sci. Instrum. **78**, 013705 (2007).

¹⁶M. Treier *et al.*, Surf. Sci. **602**, L84 (2008).

¹⁷R. Fasel *et al.*, Phys. Rev. Lett. **76**, 4733 (1996).

¹⁸C. S. Fadley, in *Synchrotron Radiation Research: Advances in Surface Science*, edited by R. Z. Bachrach (Plenum, New York, 1990), p. 421.

¹⁹R. Fasel *et al.*, Phys. Rev. B **50**, 14516 (1994).

²⁰See EPAPS Document No. E-PRBMDO-80-R13932 for additional details on the SSC simulations. For more information on EPAPS, see <http://www.aip.org/pubservs/epaps.html>.

²¹J. F. Moulder, W. F. Stickle, P. E. Sobol, and K. D. Bomben, *Handbook of X-ray Photoelectron Spectroscopy* (Perkin-Elmer Corp., Eden Prairie, MN, 1992).

²²P. Kruger *et al.*, Surf. Sci. **601**, 3952 (2007).

²³P. Kruger *et al.*, Phys. Rev. Lett. **100**, 055501 (2008).

²⁴F. Bondino *et al.*, J. Phys. Chem. B **110**, 7289 (2006).

²⁵A. Fohlich *et al.*, Nature (London) **436**, 373 (2005).

²⁶S. Stevenson *et al.*, Inorg. Chem. **47**, 1420 (2008).

²⁷S. Stevenson *et al.*, Chem. Eur. J. **8**, 4528 (2002).

²⁸L. Dunsch and S. Yang, Small **3**, 1298 (2007).